Giant monopole resonances in nuclei near stable and drip lines

I. Hamamoto,[1] H. Sagawa,[2] and X. Z. Zhang[1,3]
[1]*Department of Mathematical Physics, Lund Institute of Technology at University of Lund, Lund, Sweden*
[2]*Center for Mathematical Sciences, University of Aizu, Ikki-machi, Aizu-Wakamatsu, Fukushima 965, Japan*
[3]*Institute of Atomic Energy, Beijing, The People's Republic of China*
(Received 28 July 1997)

Isoscalar and isovector monopole responses of Ca isotopes towards drip lines are studied in comparison with those of stable nuclei, ^{40}Ca, ^{90}Zr, and ^{208}Pb, using the self-consistent Hartree-Fock calculation plus the random phase approximation with Skyrme interactions. Including simultaneously both the isoscalar and the isovector correlation the RPA response function is calculated in the coordinate space so as to take properly into account the continuum effect. The distribution of the monopole strength is much affected by the presence of the low-energy threshold strength in both proton and neutron drip line nuclei, while the isoscalar monopole strength is concentrated in one giant peak in the heavy β-stable nucleus ^{208}Pb. It is found that in drip line nuclei the transition density and the displacement field of protons are very different from those of neutrons, especially around the nuclear surface. The relation between the compression modulus of the nuclear matter K_{nm} and that of finite nuclei K_A is also discussed by using the energy moments estimated in RPA. [S0556-2813(97)04412-9]

PACS number(s): 24.30.Cz, 21.10.Re, 21.60.Ev, 21.60.Jz

I. INTRODUCTION

The structure of nuclei far from β stability is an exciting research field, since a number of new phenomena are expected or have been observed in connection with the small binding energies of the least bound nucleons as well as the unusual ratio between the number of protons and that of neutrons. Among various nuclear excitations, giant monopole resonance (GMR), the so-called ''breathing mode,'' is particularly interesting because of its relation with the nuclear matter compression modulus K_{nm}. The compression modulus is defined by the second derivative of the energy at the saturation point of nuclear matter,

$$K_{nm}=\left[9\rho^2\frac{d^2(E/A)}{d\rho^2}\right]_{\rho=\rho_0}=\left[k^2\frac{d^2(E/A)}{dk^2}\right]_{k=k_F} \quad (1)$$

where $\rho_0(k_f)$ is the equilibrium density (Fermi momentum) and E/A is the nuclear matter energy. The isoscalar giant monopole resonances (IS GMR) are observed in various experiments which led to a value of nuclear matter compression modulus $K_{nm}\approx(210\pm30)$ MeV in the early 1980s [1–4]. After the systematic studies, it was claimed [5] that the new data allow a better separation between the surface and the volume term in the expression of the compression moduli and lead consequently to a new value $K_{nm}\approx(300\pm25)$ MeV which is significantly larger than the one that was obtained in the earlier systematic analysis.

The isovector GMR (IV GMR) has also been a subject of intensive study in relation to the bulk properties of nuclei, i.e., the symmetry energy coefficient and the compression modulus. To what extent the symmetry energy and/or the compression modulus affect the excitation energy and the transition strength of the IV GMR is an interesting question. The IV GMR also has an important effect on the breaking of the isospin symmetry in nuclei [6]. Quantitative information on IV GMR is highly desired for a realistic estimate of the isospin mixing in nuclei.

In this paper, we study the IS and the IV GMR by using a self-consistent Hartree-Fock (HF) plus the random phase approximation (RPA). As effective interactions, the same Skyrme interactions are used in both HF and RPA calculations and no other parameters are introduced in our present study [7,8]. It is the prime advantage of the self-consistent model that the nuclear compression moduli will be directly compared with the excitation spectra of the monopole response [9,10]. The RPA response function is solved in the coordinate space with the proton-neutron formalism including simultaneously both the IS and the IV correlation [8]. In this way, we can take properly into account the coupling to the continuum and the effect of neutron (proton) excess on the structure of the giant resonances in nuclei near the neutron (proton) drip lines.

The dynamical structure of excitation modes can be studied from the transition density and the displacement field. A nuclear state at a given energy in the continuum can contain contributions from many excitations modes with different dynamical structure. Thus, for example, the neutron part of the IS monopole transition density at a given energy may possibly be different from that of the IV monopole transition density at the same energy. Our model can naturally produce this difference if it exists [8,11]. In contrast, if a continuum state at a given energy is obtained by the expansion of oscillator bases and, thus, is expressed as an isolated quantum state, the difference does not exist. In the quadrupole responses studied in Refs. [8,11] the neutron (proton) part of the IS transition density is nearly equal to that of the IV transition density at the same energy, almost whenever an appreciable amounts of both the IS and the IV quadrupole strength are found at the energy. It is interesting to consider whether or not this is also the case for monopole responses.

Basic formulas including various ways to define GMR energies and the nuclear compression modulus K_A are summarized in Sec. II. In Sec. III, we discuss HF+RPA results of stable nuclei ^{40}Ca, ^{90}Zr, and ^{208}Pb by using three different Skyrme interactions SkM*, SGI, and SIII. The three interactions have different nuclear compression moduli in nuclear matter: $K_{nm}=217$, 256, and 355 MeV for SkM*, SGI, and SIII, respectively. Among realistic effective interactions that give reasonable binding energies and mean square radii for the ground states of stable nuclei, the SkM* and the SIII interactions are two extremes that have a small and a large compression modulus, while the SGI interaction has a medium value of the compression modulus. In Sec. IV the result of several Ca isotopes, ^{34}Ca, ^{40}Ca, ^{48}Ca, and ^{60}Ca, is presented in order to study the exotic properties of the monopole response in nuclei near both the proton and the neutron drip lines. In Sec. V we illustrate the possible difference between the neutron (or proton) part of the IS transition density and that of the IV transition density at a given energy in the continuum, showing numerical examples. A summary is given in Sec. VI.

II. MODEL AND FORMULATION

We perform the self-consistent HF+RPA calculations to study the GMR with Skyrme interactions. First, the HF equation is solved in the coordinate space by using the Numerov algorithm. Then, the RPA response function $G_{\rm RPA}$ is solved in the coordinate space and the strength distributions $S(E)$ are obtained from the imaginary part of $G_{\rm RPA}$ as

$$S(E)=\sum_n |\langle n|Q|0\rangle|^2\delta(E-E_n)$$
$$=\frac{1}{\pi}\,\mathrm{Im}\,\mathrm{Tr}(Q^\dagger(\vec r)G_{\rm RPA}(\vec r,\vec r';E)Q(\vec r')), \qquad (2)$$

where Q expresses one-body operators

$$Q^{\lambda=0,\tau=0}=\frac{1}{\sqrt{4\pi}}\sum_i r_i^2 \quad \text{for isoscalar monopole strength} \qquad (3)$$

and

$$Q^{\lambda=0,\tau=1}=\frac{1}{\sqrt{4\pi}}\sum_i \tau_{zi}r_i^2 \quad \text{for isovector monopole strength.} \qquad (4)$$

The transition density for an excited state, $|n\rangle$,

$$\rho^{tr}_{n0}(\vec r)\equiv\langle n|\sum_{i=1}^{A}\delta(\vec r-\vec r_i)|0\rangle \qquad (5)$$

can be obtained from the RPA response, since the imaginary part of the $G_{\rm RPA}(\vec r,\vec r';E_n)$ near the resonance is proportional to $\rho^{tr}_{n0}(\vec r)\rho^{tr}_{n0}(\vec r')^\dagger$. The reduced transition probability is calculated using the transition density in Eq. (5) as

$$B(\lambda=0,\tau:0\to n)=\left|\int \rho^{tr}_{n0}(\vec r)Q^{\lambda=0,\tau}d^3r\right|^2, \qquad (6)$$

where the excited state denoted by n has the angular momentum ($\lambda=0$). The radial transition density, $\rho^{tr}_\lambda(r)$, is defined by

$$\rho^{tr}_{n0}(\vec r)\equiv\rho^{tr}_\lambda(r)Y_{\lambda\mu}(\hat r). \qquad (7)$$

The calculated RPA transition densities may be compared with two kinds of transition densities of collective models. The radial transition density by Tassie has the radial dependence

$$\rho^{tr}_{\rm Tassie}(r)=\alpha\left(3\rho_0+r\,\frac{d\rho_0}{dr}\right), \qquad (8)$$

where α is a constant and ρ_0 is the ground state density. The radial transition density of the simplest version of the hydrodynamical polarization model may be written [12] as

$$\rho^{tr}_{\rm pol}(r)=\alpha'\rho_0(r)j_0(kr), \qquad (9)$$

where α' is a constant and the $j_0(kr)$ is the spherical Bessel function. The value k in Eq. (9), $k=4.4934/1.2A^{1/3}$, is determined by the boundary condition for the velocity field at the nuclear surface. We note that in Ref. [12] $\rho_0(r)$ was independent of r due to the assumption of the hydrodynamical model.

Using the calculated HF ground state density $\rho_0(r)$, and the radial transition density, $\rho^{tr}(r)$, we further study the displacement field [1] defined by

$$u(r)=-\frac{1}{r^2\rho_0(r)}\int_0^r R^2\rho^{tr}(R)dR, \qquad (10)$$

which is derived by using the continuity equation. If the Tassie transition density (8) is used for ρ^{tr} in Eq. (10), the displacement field $u(r)$ is simply proportional to r.

The excitation energy of GMR is often calculated by using the energy moment of the transition strength,

$$m_k^\tau=\sum_n (E_n)^k|\langle n|Q^{\lambda=0,\tau}|0\rangle|^2, \qquad (11)$$

where n denotes the RPA state. The IS GMR energy referred to as the scaling energy is defined by

$$E_0^s=\sqrt{m_3^{\tau=0}/m_1^{\tau=0}}. \qquad (12)$$

The energy (12) is particularly interesting for the discussion of the compression modulus since the scaling hypothesis for the isoscalar monopole vibration yields [2] the following relation between E_0^s and the nuclear compression modulus K_A^s:

$$K_A^s=\frac{m(E_0^s)^2\langle r^2\rangle_m}{\hbar^2} \qquad (13)$$

where $\langle r^2\rangle_m$ is the mean mass squared radius. There are other ways to define the energy of GMR by using the moments m_k^τ. The average energy E is defined by

$$\overline{E} = m_1^\tau / m_0^\tau , \tag{14}$$

which is close to the peak energy of GMR, if it is a single peak. The IS GMR energy may also be defined by

$$E_0^c = \sqrt{m_1^{\tau=0} / m_{-1}^{\tau=0}}. \tag{15}$$

The energy (15) has a direct relation with the compression modulus K_A^c which is derived from the constrained HF calculation with the nuclear radius parameter [1]

$$K_A^c = \left[R^2 \frac{d^2(E/A)}{dR^2} \right]_{R=R_0} = \frac{2A\langle r^2 \rangle_m^2}{m_{-1}^{\tau=0}} = \frac{m(E_0^c)^2 \langle r^2 \rangle_m}{\hbar^2}, \tag{16}$$

where $R_0^2 = \langle r^2 \rangle_m$ and E/A is the HF energy.

For the IV GMR we use the notations

$$\overline{E_3} = \sqrt{m_3^{\tau=1} / m_1^{\tau=1}} \tag{17}$$

and

$$\overline{E_1} = \sqrt{m_1^{\tau=1} / m_{-1}^{\tau=1}}, \tag{18}$$

which correspond to the quantities, (12) and (15), for the IS GMR, respectively.

The variance

$$\sigma = \sqrt{m_2/m_0 - (m_1/m_0)^2} \tag{19}$$

is a measure of the width of the GMR in the present calculations. If the strength distribution has a Gaussian shape, the width $\Gamma_{\rm FWHM}$ has a relation $\Gamma_{\rm FWHM} = 2.35\sigma$. In most cases the RPA strength distribution shows many small peaks beside the main giant resonance peak so that the value of σ is not directly related to $\Gamma_{\rm FWHM}$, but it gives a rough measure of the dispersion of the calculated strength distribution. Though the particle escape width is fully taken into account in the present calculations, the calculated widths may not be directly compared with measured widths, since the spreading width due to the coupling to nearby complicated configurations is not included.

The relation between K_A and K_{nm} is often discussed using an analogy with the expression of the semi-empirical mass formula. The nuclear compression modulus may be expressed in terms of the volume, the surface, the symmetry, and the Coulomb contributions,

$$K_A = K_{\rm vol} + K_{\rm surf} A^{-1/3} + K_{\rm sym} \left(\frac{N-Z}{A} \right)^2 + K_{\rm Coul} \frac{Z^2}{A^{4/3}} + \cdots . \tag{20}$$

Other terms such as a curvature term or a surface symmetry term are also considered in Refs. [1,4]. The various terms in Eq. (20) are determined by fitting experimental IS GMR energies. Then, the nuclear matter compression modulus K_{nm} may be identified as the volume term $K_{\rm vol}$ in the limit of $A \to \infty$, which is the case when the giant monopole vibration is described by the scaling model of the ground state density [4,10]. However, the relation between K_{nm} and $K_{\rm vol}$ depends indeed on the model used. Defining the asymptotic limit of the compression modulus by using a parameter α_K,

$$\lim_{A \to \infty} K_A = K_{\rm vol} = \alpha_K K_{nm} . \tag{21}$$

The value of α_K is equal to 1 for the scaling model. On the other hand, the constrained deformed density for the monopole vibration gives $\alpha_K = 7/10$ [13], while the hydrodynamical model gives $\pi^2/15$ [3].

III. GMR IN β-STABLE NUCLEI

Giant monopole resonances in β-stable nuclei have been previously calculated in many publications, using various theoretical models. It is often stated that the calculated giant monopole resonance is not found as a single collective mode in nuclei with the mass number smaller than $A \approx 90$. The statement is in agreement with available experimental informations and also with our calculated result. On the other hand, it seems that both the monopole strength and its energy distribution in the nucleus such as ^{40}Ca, which are extracted from experiments, depend appreciably on the assumption employed in the analysis. In this section we present our calculated results of ^{40}Ca, ^{90}Zr, and ^{208}Pb, in order to be able to compare them later with those of drip line nuclei.

In Table I the result of IS GMR energies (12), (14), and (15) calculated by using SkM*, SGI, and SIII interactions, are summarized together with the nuclear compression moduli (13) and (16), the variance (19), and the HF mass radius. Due to the identity of the energy moments $m_{k+1} m_{k-1} \geqslant \underline{m_k^2}$, we have the relation $E_0^s \geqslant \overline{E} \geqslant E_0^c$. The energies E_0^s, E, and E_0^c of the IS GMR in Table I become smaller for the interaction with a smaller compression modulus K_{nm}. In contrast, the corresponding three energies $\overline{E_3}$, $\underline{E}$, and $\overline{E_1}$, of the IV GMR in Table II do not show a simple monotonic dependence on values of K_{nm}, because of the important role in IV modes played by the symmetry term. The symmetry energy coefficient a_τ is equal to 26.1, 28.5, and 28.2 MeV for the SkM*, the SGI, and the SIII interactions, respectively. The calculated energies of the IS GMR in Table I show approximately the $A^{-1/3}$ dependence when one compares the corresponding values of ^{90}Zr and ^{208}Pb, while the $A^{-1/3}$ dependence is considerably broken as one goes from ^{90}Zr to ^{40}Ca. This already indicates that the giant monopole resonances in ^{40}Ca are of different nature from those of heavier nuclei. However, it is well known that even for the well-established IV giant dipole resonances the $A^{-1/3}$ dependence does not work for nuclei with $A < 50$.

In Table I available experimental energies of the IS GMR are given, which may be taken as lower limit values, since any IS monopole strength not yet detected and lying possibly in a higher energy region, which will give the missing part of the EWSR, can increase those energies. As far as the average energies are concerned, the SkM* interaction having the compression modulus $K_{nm} = 217$ MeV gives a reasonable agreement with the available data, while the SGI and the SIII interaction predict appreciably higher energies. This conclusion agrees with that of Refs. [1,4,10], but not that of Ref. [5]. A more detailed comparison between our results and experimental data will be given for each nucleus later in the present section.

The calculated IS and IV monopole responses of ^{40}Ca are shown in Figs. 1(a) and 1(b), using the SkM*, the SGI, and

TABLE I. Properties of the IS RPA response in ^{40}Ca, ^{90}Zr, and ^{208}Pb. The energies E_0^s, $\overline{E}$, and E_0^c are defined by Eqs. (12), (14), and (15), respectively. The compression moduli K_A^s and K_A^c are defined by Eqs. (13) and (16), respectively. The variance σ is defined by Eq. (19). The last column gives the HF mass radius $\sqrt{\langle r^2\rangle_m}$. The experimental values are taken from Ref. [15] for ^{40}Ca and Ref. [17] for ^{90}Zr and ^{208}Pb.

A		E_0^s (MeV)	$\overline{E}$ (MeV)	E_0^c (MeV)	K_A^s (MeV)	K_A^c (MeV)	σ (MeV)	$\sqrt{\langle r^2\rangle_m}$ (fm)
^{40}Ca	SkM*	22.5	21.0	20.6	141.0	118.0	4.4	3.402
	SGI	24.9	23.5	23.1	168.0	145.0	4.6	3.350
	SIII	27.5	25.5	24.9	208.0	171.0	5.7	3.384
	exp.	21.3	18.9	17.3				
^{90}Zr	SkM*	19.1	18.5	18.4	160.0	148.0	2.6	4.259
	SGI	20.8	20.2	20.1	188.0	176.0	2.7	4.247
	SIII	23.2	22.4	22.2	238.0	218.0	3.3	4.289
	exp.		16.2					
^{208}Pb	SkM*	14.5	14.1	14.0	157.0	146.0	1.9	5.557
	SGI	15.7	15.4	15.4	184.0	174.0	1.8	5.569
	SIII	17.9	17.4	17.2	242.0	224.0	2.5	5.599
	exp.		13.8					

the SIII interactions, respectively. Although the structure of the IS response of ^{40}Ca in Fig. 1(a) depends on interactions used, a broad peak with a large width of about 10 MeV is always obtained. For example, the isoscalar response with the SkM* interaction shows a very broad peak around $E_x = 20$ MeV with a width of 8 MeV. This peak exhausts 79% of the IS energy weighted sum rule value (EWSR). The variance σ is the largest for the SIII interaction with $\sigma = 5.7$ MeV and the smallest for the SkM* interaction with $\sigma = 4.4$ MeV. The RPA IV monopole strength with the SkM* interaction may be divided into two energy regions, $10 < E_x < 27$ MeV and $E_x > 27$ MeV. The strength in the former region is the left-over part of the unperturbed strength which is not shifted to the higher energy region by the IV RPA correlation, as can be seen in comparison with the unperturbed response in Fig. 2. On the other hand, the strength in the latter region is the correlated IV GMR. Thus, the large value of the variance σ in Table II originates principally

TABLE II. Various energies of the IV RPA response in ^{40}Ca, ^{90}Zr, and ^{208}Pb. The energies $\overline{E_3}$, $\overline{E}$, and $\overline{E_1}$ are defined by Eqs. (17), (14), and (18), respectively. The variance σ is defined by Eq. (19).

A		$\overline{E_3}$ (MeV)	$\overline{E}$ (MeV)	$\overline{E_1}$ (MeV)	σ (MeV)
^{40}Ca	SkM*	35.7	31.4	29.7	9.7
	SGI	38.7	34.4	32.7	10.2
	SIII	38.0	33.5	31.6	10.4
^{90}Zr	SkM*	33.3	31.0	30.0	7.8
	SGI	35.3	32.8	31.8	7.6
	SIII	35.0	32.3	31.2	7.8
^{208}Pb	SkM*	28.3	25.7	24.4	7.0
	SGI	29.6	27.2	26.1	6.8
	SIII	29.8	27.1	25.6	7.4

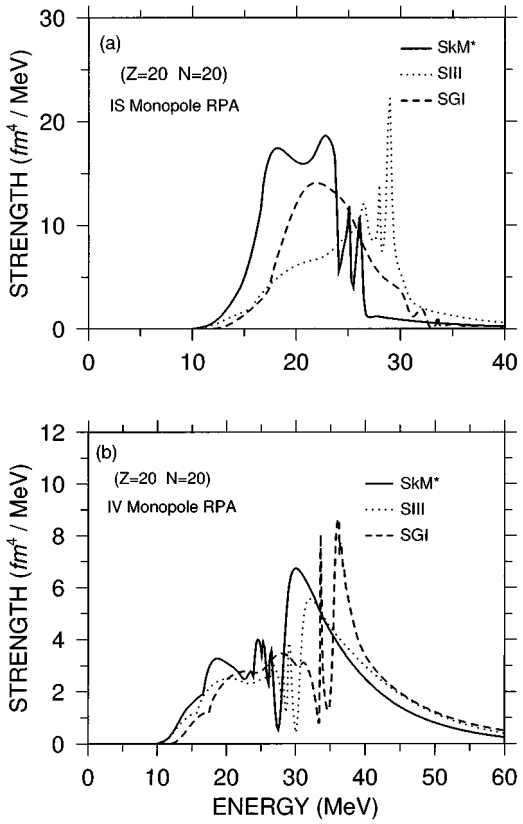

FIG. 1. RPA monopole strength function of ^{40}Ca as a function of excitation energy: (a) IS response; (b) IV response. The results with the SkM*, the SIII, and the SGI interaction are shown by solid, dotted, and dashed curves, respectively.

from the presence of the uncorrelated unperturbed strength and does not really mean the large variance of the correlated IV GMR.

The energy E_0^s of the IS monopole with the SkM* interaction is 22.5 MeV, which is substantially smaller than those

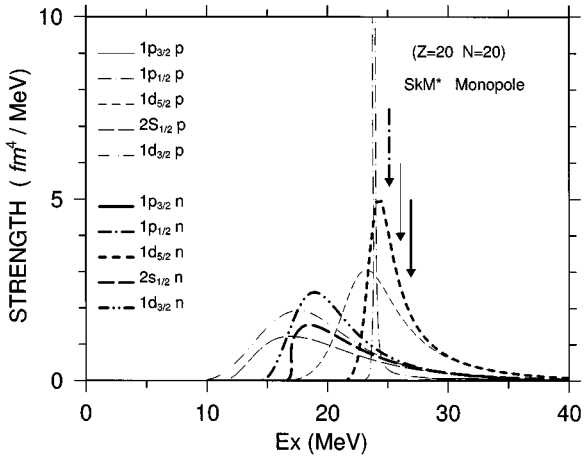

FIG. 2. Unperturbed response connected with excitations of protons or neutrons in a given orbital of ^{40}Ca. The SkM* interaction is used. Arrows indicate the positions of the unperturbed strength with either vanishing width (i.e., excitations to bound particle states) or very small width (i.e., excitations to very sharp resonant particle states).

with the SGI and the SIII interaction, 24.9 MeV and 27.5 MeV, respectively. There are two sets of experimental data available for IS GMR in ^{40}Ca. The (α,α') data of Groningen group [14] observed monopole strength at around $E_x = 14.4$ MeV, which exhausts $(30\pm6)\%$ of EWSR. Recent experimental data [15] obtained by inelastic scattering of α particles suggest the presence of $(92\pm2)\%$ of the isoscalar monopole EWSR in the energy region of $E_x = 7.5-28.8$ MeV with a centroid of 18.9 ± 0.4 MeV and a width of 11.1 MeV. The empirical values of E_0^s and E_0^c in this energy range are $E_0^s(\text{expt.})=(21.3\pm0.12)$ MeV and $E_0^c(\text{expt.})=(17.29\pm0.12)$ MeV, respectively, which are closer to the calculated values with the SkM* interaction than those with the SGI or the SIII interaction.

The unperturbed response connected with excitations of particles in a given occupied orbital of ^{40}Ca is shown in Fig. 2, calculated in the HF potential with the SkM* interaction. The three arrows indicate the p-h excitations to a sharp resonance $(1p_{3/2}\rightarrow 2p_{3/2})_p$, and to bound particle states $(1p_{1/2}\rightarrow 2p_{1/2})_n$ and $(1p_{3/2}\rightarrow 2p_{3/2})_n$, of which the strength can be estimated from the pole of the real part of the response (2). The neutron strength just above each threshold energy E_{thr} rises as $(E_x-E_{\text{thr}})^{l+1/2}$ [16]. Thus, the strength with the $(2s_{1/2})_n$ hole orbit increases very quickly, while the one with the $(1d_{5/2})_n$ and $(1d_{3/2})_n$ hole orbits increases moderately just above respective thresholds. The behavior of the threshold strength is quite different for proton excitations due to the presence of the Coulomb barrier. The total unperturbed strength is distributed over a wide energy range from $E_x=10$ to 30 MeV, and the IS RPA correlation shifts down only slightly the position of the broad peak. Moreover, the escape widths of some p-h configurations are as large as 5–7 MeV and could contribute substantially to the width of the RPA response.

In Fig. 3(a) we show the IS transition densities of ^{40}Ca at the peaks $E_x=18.0$ MeV and 22.5 MeV in Fig. 1(a). The transition densities are normalized to have $B(\lambda=0)=34.0$ fm^4 for the peak at $E_x=18.0$ MeV and $B(\lambda=0)=29.6$ fm^4 for the peak at $E_x=22.5$ MeV. These $B(\lambda=0)$ values are obtained by integrating the response $S(E)$ in Fig. 1(a) in the energy interval of $E_x\pm2$ MeV. The RPA transition density at $E_x=18.0$ MeV shows a typical IS character where the neutron and the proton densities are identical. The transition density at $E_x=22.5$ MeV has also a strong IS character showing only a minor difference between the proton and the neutron densities. The Tassie density is normalized to have $B(\lambda=0)=34.0$ fm^4 which is the same as that of the transition density at $E_x=18$ MeV. There is a substantial difference of the radial dependence between the Tassie density and the density at $E_x=18$ MeV, especially around the surface, while the density at $E_x=22.5$ MeV has the radial dependence similar to that of Tassie.

The IV transition density at $E_x=30$ MeV with the SkM* interaction is shown in Fig. 3(b). The absolute magnitude of the transition density is normalized to be $B(\lambda=0)=64.6$ fm^4, which is the value obtained by integrating the response strength over the region of $E_x=28-45$ MeV. The transition densities in Fig. 3(b) show a typical IV character, the same magnitude for protons and neutrons with opposite signs. Compared with the Tassie density, the RPA transition density has a node at a larger radius and a much longer tail.

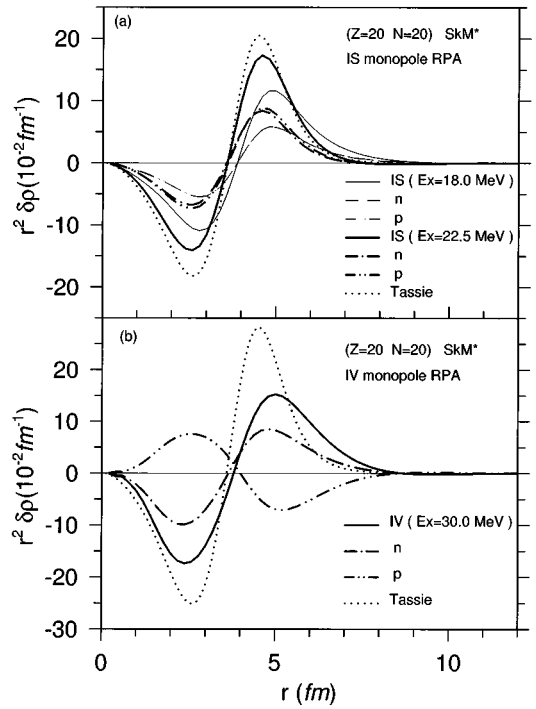

FIG. 3. (a) Radial transition densities of IS GMR in ^{40}Ca calculated at $E_x=18.0$ and 22.5 MeV, as a function of radial coordinate. The neutron part is expressed by dot-dashed lines, while the proton part is denoted by dot-dot-dashed lines. The IS density is expressed by solid lines. The Tassie density for GMR (8) is also given by the dotted line, which is normalized so as to give the same $B(\lambda=0)$ value as that of the IS density at $E_x=22.5$ MeV. (b) Radial transition densities of IV GMR in ^{40}Ca calculated at $E_x=30$ MeV. The IV density is denoted by the solid line.

The IS and the IV monopole response in ^{90}Zr are given in Figs. 4(a) and 4(b) for the three interactions, SkM*, SGI, and SIII. Compared with ^{40}Ca, it is seen that the IS response in the heavier nucleus ^{90}Zr shows a tendency to form a narrow single peak of GR. The variance σ of IS GMR in ^{90}Zr is almost a half of that in ^{40}Ca, as shown in Table I.

The experimental data of IS GMR in ^{90}Zr are reported in Refs. [17,18,19]. The peak energy is identified to be 16.20 ± 0.50 MeV, 16.10 ± 0.28 MeV, and 16.40 ± 0.25 MeV in Refs. [17,18,19], respectively, while the transition strength exhausts $(90\pm20)\%$ in Ref. [17] and 39% in Ref. [19] of the IS EWSR. There is no quantitative assessment of the strength in Ref. [18]. In order to confirm the IS GMR strength in ^{90}Zr, especially the sum rule strength, it is desirable to study quantitatively the monopole strength in the energy region higher than the presently available data.

In the RPA IV response with the SkM* interaction of Fig. 4(b) the major part of the strength in the region of $E_x<26$ MeV is the leftover unperturbed strength, without being shifted to a higher energy region by the IV RPA correlation, while the strength at $E_x>26$ MeV expresses the IV GMR. The small shoulder at 17.8 MeV, which is seen on the bump of the leftover unperturbed strength, is the IV strength associated with the IS GMR due to the presence of the neutron excess. The ratio of this associated IV strength to the IS strength at the IS GMR is much smaller than that of the IV

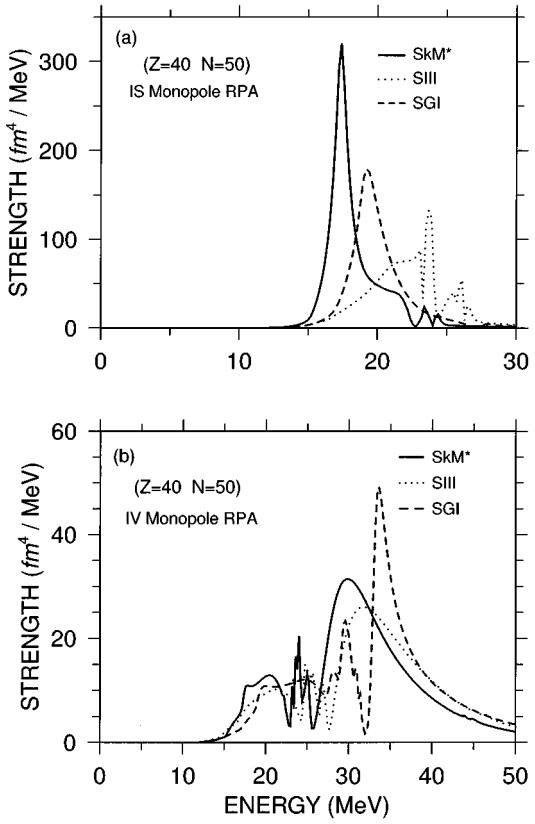

FIG. 4. RPA monopole strength function of ^{90}Zr as a function of excitation energy: (a) IS response; (b) IV response. The results with the SkM*, the SIII, and the SGI interaction are shown by solid, dotted, and dashed curves, respectively.

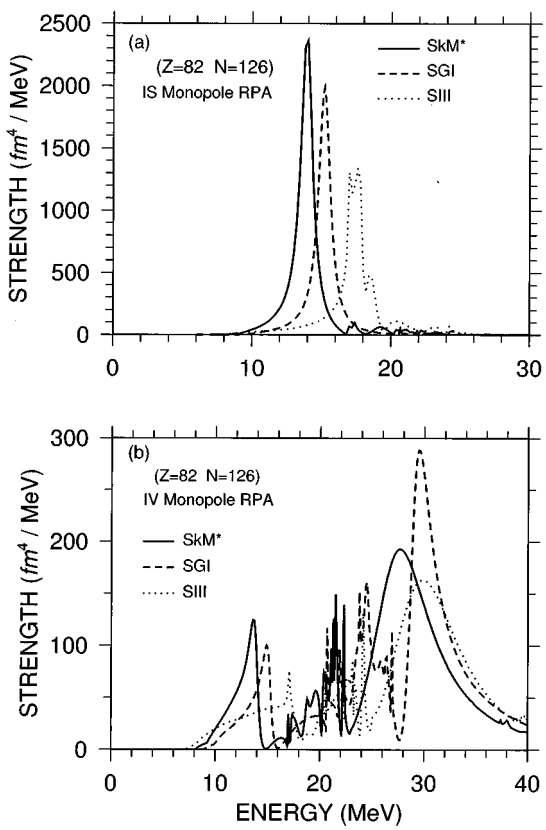

FIG. 5. RPA monopole strength function of ^{208}Pb as a function of excitation energy: (a) IS response; (b) IV response. The results with the SkM*, the SIII, and the SGI interaction are shown by solid, dotted, and dashed curves, respectively.

quadrupole strength to the IS strength at the IS giant quadrupole resonance (GQR) due to the same neutron excess [8].

The IS and the IV monopole strength in ^{208}Pb are given in Figs. 5(a) and 5(b) for the SkM*, the SGI, and the SIII interactions. The IS response in Fig. 5(a) for all three interactions shows, in a good approximation, a single peak with the width of about 1 MeV. The peaks for the SkM* and the SGI interaction exhaust about 91% of the EWSR. The IS peak of the SIII interaction around $E_x=17$ MeV exhausts only 71% of the EWSR. The IV GMR is seen as the peak in Fig. 5(b) in the region of $E_x>23$, 25, and 28 MeV for the SkM*, the SGI, and the SIII interaction, respectively. Though the IV strength associated with the IS GMR due to the neutron excess is clearly seen at the peak energy of the respective IS GMR for the three Skyrme interactions, the ratio of the associated IV strength to the IS strength at the IS GMR is in fact much smaller than the value of $(N-Z)/A$. See Ref. [8] for the corresponding ratio in the case of the GQR.

The IS GMR in ^{208}Pb is experimentally best explored among IS GMR in various nuclei. The (α,α') data were reported to show a peak at $E_x=13.70\pm0.40$ MeV exhausting (90 ± 20)% of the EWSR value [17]. Another (α,α') data give the peak energy at $E_x=13.90\pm0.30$ MeV [20]. The (^{3}He,^{3}He$'$) data [19] give almost the same result; the energy of the peak is $E_x=13.20\pm0.30$ MeV, which consumes 92% of the EWSR value. These data agree well with the calculated peak at $E_x=13.9$ MeV using the SkM* interaction.

The IS and the IV transition densities are shown in Figs. 6(a) and 6(b) for the SkM* interaction. The transition densities of the IS peak at $E_x=13.75$ MeV, having $B(\lambda=0)=3259$ fm^4, are shown in Fig. 6(a) together with the Tassie density in Eq. (8). Although the radial dependence of the density of neutrons and that of protons are appreciably different, especially in the region of $r=6-10$ fm, the sum of those two, namely the IS transition density, shows a radial dependence similar to that of the Tassie. The transition densities of IV GMR at $E_x=27.6$ MeV are shown together with the Tassie in Eq. (8) and the polarization density in (9). The $B(\lambda=0)$ value of this IV peak is 1453 fm^4. The RPA IV density has almost equal contributions from neutrons and protons with a small difference around the node points, and a tail much longer than the Tassie or the polarization densities.

In Fig. 6(c) we show the displacement field (10) calculated at the peak energy of the IS GMR in ^{208}Pb. It is seen that the displacement field of protons behaves nearly in the same way as that of neutrons does. For reference, the displacement field calculated numerically by using the Tassie transition density is plotted, in which the Tassie density is normalized so as to give the same $B(\lambda=0)$ value.

Using the SkM* interaction, in Fig. 7 we show the unperturbed response, the IS RPA response with the simultaneous inclusion of the IS and the IV correlation (the solid curve), and the RPA response including only the IS part of the interaction (the dashed curve). The IS GMR in ^{208}Pb is shifted very clearly downwards from the energy region of the unper-

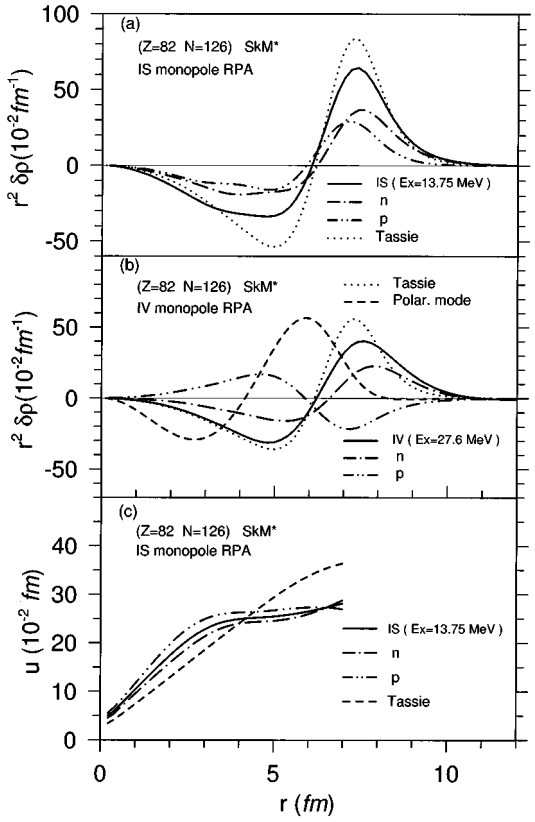

FIG. 6. (a) Radial transition densities of IS GMR in ^{208}Pb calculated at $E_x = 13.75$ MeV, as a function of radial coordinate. The neutron part is expressed by the dot-dashed line, while the proton part is denoted by the dot-dot-dashed line. The IS density is expressed by the solid line. The Tassie density for GMR (8) is also given by the dotted curve, which is normalized so as to give the same $B(\lambda=0)$ value as that of the IS density. (b) Radial transition densities of IV GMR in ^{208}Pb calculated at $E_x = 27.6$ MeV. The IV density is expressed by the solid line. The Tassie and the polarization densities for GMR, (8) and (9), which are normalized so as to give the same $B(\lambda=0)$ value as that of the IV density, are also shown by the dotted and the dashed curves, respectively. (c) The displacement field (10) calculated at the peak energy, $E_x = 13.75$ MeV, of the IS GMR in ^{208}Pb. For reference, the displacement field, which is numerically calculated using the Tassie transition density, is plotted by the dashed line. The Tassie transition density is normalized so as to give the same $B(\lambda=0)$ value as that of the plotted IS transition density.

turbed strength, while in much lighter nuclei such as ^{40}Ca the IS GMR lies nearly in the same energy region as that of the unperturbed strength. This leads to the difference in which the IS GMR is nearly a narrow single peak in ^{208}Pb, while in ^{40}Ca the IS GMR is not found as a single collective peak. The peak energy $E_x = 13.75$ MeV for the full calculation is 500 keV higher than that of the dashed curve, since the inclusion of the IV correlation places the small IV strength (due to the neutron excess) at the IS GMR and, at the same time, makes the energy of the IS GMR higher.

In Fig. 8, the calculated compression moduli K_A^s and K_A^c are plotted as a function of mass number A. The figure is similar to Fig. 2 of Ref. [4]. The compression moduli are nearly constant as one goes from ^{90}Zr to ^{208}Pb, and whether

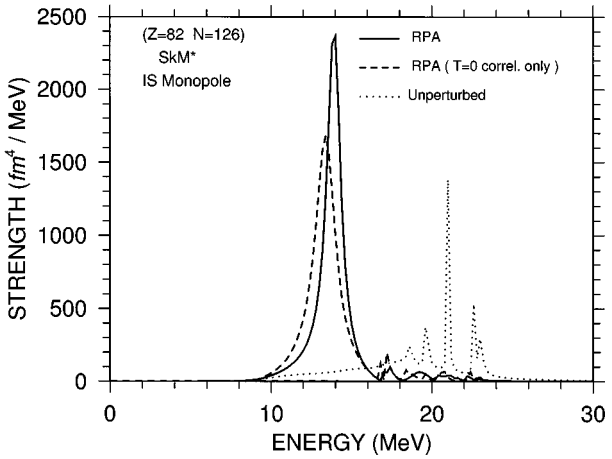

FIG. 7. RPA monopole strength function of ^{208}Pb with the SkM* interaction as a function of excitation energy. The IS strength estimated in RPA, in which both the IS ($T=0$) and the IV ($T=1$) correlations are simultaneously taken into account, is shown by solid curves, while the one in which only the IS ($T=0$) correlation is included is plotted by dashed curves. The unperturbed strength is denoted by the dotted curve.

they slightly increase or decrease may depend on the Skyrme interactions used.

From the RPA results in Table I and Fig. 9, the compression modulus K_A^s is related to K_{nm} as

$$K_A^s = 35 + 0.49K_{nm} \quad (^{40}\mathrm{Ca}),$$

$$K_A^s = 38 + 0.57K_{nm} \quad (^{90}\mathrm{Zr}),$$

$$K_A^s = 23 + 0.62K_{nm} \quad (^{208}\mathrm{Pb}). \tag{22}$$

The above expression for ^{40}Ca may not be so meaningful, since the IS GMR is not obtained as a single collective peak. There is a mass number dependence of the coefficient in front of K_{nm} obtained numerically from RPA calculations. The largest value of the coefficient is obtained for ^{208}Pb, while for ^{40}Ca and ^{90}Zr it is 10–20 % smaller than that of ^{208}Pb. Moreover, in Eq. (22) we have obtained a nonzero

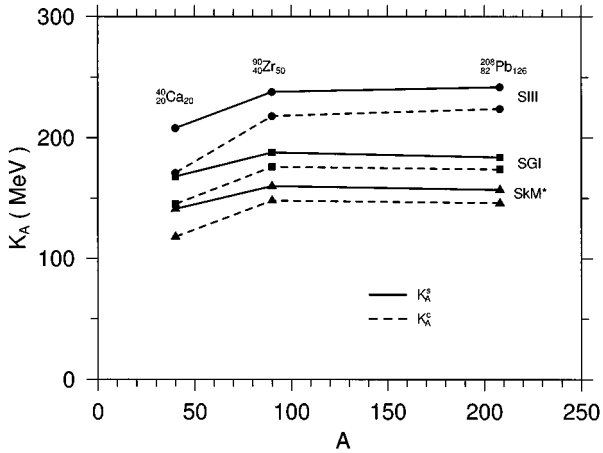

FIG. 8. Calculated nuclear compression moduli K_A^s in Eq. (13) and K_A^c in Eq. (16) as a function of mass number.

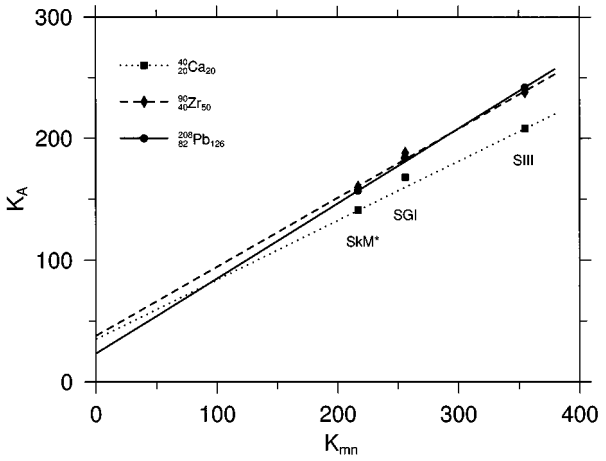

FIG. 9. The compression modulus K_A^s in Eq. (13) as a function of the nuclear matter compression modulus K_{nm}.

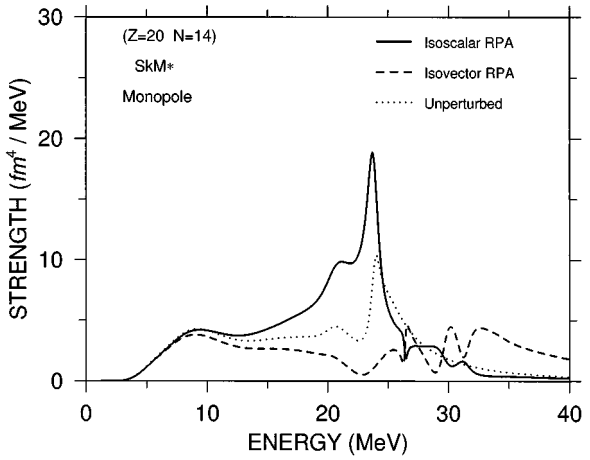

FIG. 10. RPA monopole strength function of ^{34}Ca as a function of excitation energy. The SkM* interaction is used consistently both in the HF and the RPA calculations. The IS (IV) response is shown by the solid (dashed) curve, while the unperturbed response is denoted by the dotted curve.

constant term, compared with the expression (21). The presence of this nonzero constant term suggests that even ^{208}Pb is not large enough to obtain a relation between K_A^s and K_{nm} in the limit of $A\rightarrow\infty$. The obtained α_K value for ^{208}Pb approaches the hydrodynamical value of $\alpha_K=\pi^2/15=0.658$. However, this might be just accidental since there is no similarity between the transition density of the RPA IS GMR and that of the hydrodynamical polarization model.

The hydrodynamical polarization model [12] predicts the excitation energy of IV GMR in nuclei with $Z=N$ to be

$$E_x=170A^{-1/3}\ \text{MeV}. \tag{23}$$

The average energies $\overline{E_3}$ for ^{208}Pb in Table II happen to be very close to the value given by Eq. (23). On the other hand, the $\overline{E_3}$ values for ^{40}Ca and ^{90}Zr are considerably smaller than the estimate in Eq. (23).

IV. GMR IN Ca-ISOTOPES NEAR DRIP LINES

In this section we mainly discuss the numerical results obtained by using the SkM* interaction, since in the preceding section the comparison of the calculated GMR properties of β-stable nuclei with experimental data favors the SkM* interaction having the low compression modulus $K_{nm}=217$ MeV. In the following it is seen that in all Ca isotopes the IS GMR lies in the energy region of the unperturbed strength and, thus, is not found as a single collective peak, while the RPA IV strength is divided into the higher-lying IV GMR and the remaining unperturbed strength. The characteristic feature of drip line nuclei is the presence of an appreciable amount of the very low-lying unperturbed threshold strength, which can hardly be affected by the RPA correlation.

In Fig. 10, the IS and the IV monopole responses of ^{34}Ca are shown together with the unperturbed response. Both the IS and the IV response have a large bump at $E_x\approx 5-13$ MeV, which is nearly equal to the strength of unperturbed proton excitations. A prominent difference between the IS RPA response and the unperturbed strength is seen only in the region of $16<E_x<25$ MeV. Even in this energy region the shape of the IS RPA response is clearly affected by the underlying unperturbed strength. The low energy bump at $E_x=5-13$ MeV exhausts 9.4% of the EWSR, while the high energy peak $E_x=19-25$ MeV contains 51% of the EWSR. In contrast to the case of GQR [11], no IV strength due to the proton excess is brought to the energy region (i.e., $19<E_x<25$ MeV) of the IS GMR by the RPA correlation. The IV GMR may be identified as a high energy peak above $E_x=32$ MeV.

The IS transition densities of ^{34}Ca at several excitation energies are shown in Figs. 11(a) and 11(b). The $B(\lambda=0)$ values used in the normalization of the transition densities are 8.2, 8.8, and 28.4 fm^4 for $E_x=9.0$, 15.0, and 21.2 MeV, respectively. As is seen in Fig. 11(b), the transition densities at $E_x=9$ and 15 MeV are predominantly the proton densities. The transition density at $E_x=9$ MeV has a much larger tail than that at $E_x=15$ MeV, since proton holes with less binding energies are involved in the former than in the latter. The IS transition density of the high energy peak at $E_x=21.2$ MeV consists of a comparable amount of the proton and the neutron contributions, and the radial dependence is rather similar to the plotted Tassie transition density, which is normalized to have the same $B(\lambda=0)$ values as the one at $E_x=21.2$ MeV. When the transition densities in Figs. 11(a) and 11(b) are compared, we notice the shape difference: for those at lower energies the node occurs at larger r values and a larger tail is extended up to far outside of the nuclear surface. In Fig. 11(c) we show the displacement field, Eq. (10), calculated at an energy of the threshold strength, $E_x=6.5$ MeV. It is seen that the displacement field of protons is negligible inside of the nucleus and is steeply rising outside, while that of neutrons is negligible everywhere. For reference, the displacement field calculated numerically by using the Tassie transition density is plotted, in which the Tassie density is normalized so as to give the same $B(\lambda=0)$ value.

In Fig. 12 the RPA response of ^{60}Ca is shown together with the unperturbed strength. The characteristic feature of the figure looks formally very similar to that of Fig. 10 for ^{34}Ca, except for the fact that in ^{60}Ca the threshold strength

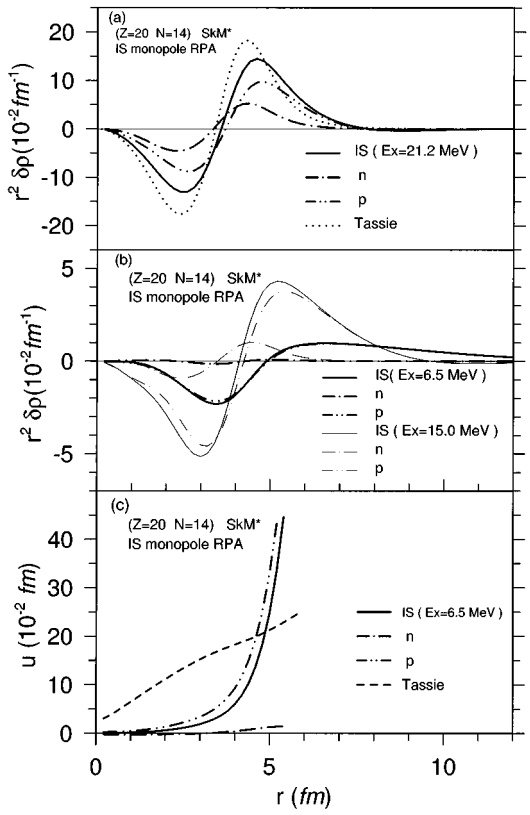

FIG. 11. Radial transition densities of the IS response in ^{34}Ca as a function of radial coordinate: (a) at an energy $E_x=21.2$ MeV, which is inside of the broad bump of the IS GMR; (b) at energies $E_x=6.5$ and 15 MeV, which are much lower than that of the IS GMR. The SkM* interaction is used. The neutron part is shown by dot-dashed lines, while the proton part is denoted by dot-dot-dashed lines. The IS density is expressed by solid lines, while the Tassie density for GMR (8) by the dotted curve in (a), which is normalized so as to give the same $B(\lambda=0)$ value as that of the IS density at $E_x=21.2$ MeV. (c) The displacement field (10) calculated at an energy of the threshold strength, $E_x=6.5$ MeV. For reference, the displacement field, which is numerically calculated using the Tassie transition density, is plotted by the dashed line. The Tassie transition density is normalized so as to give the same $B(\lambda=0)$ value as that of the plotted IS transition density at $E_x=6.5$ MeV.

consists of neutron excitations: Both the IS and the IV response has a large bump at $E_x\approx 4-12$ MeV, which is almost equal to the unperturbed neutron strength. A prominent difference between the RPA IS response and the unperturbed strength is found only in the energy region of $14<E_x<22$ MeV. The IV GMR may be identified as a high energy peak above $E_x=28$ MeV. A clear difference from Fig. 10 for ^{34}Ca is the presence of a small but clear IV strength peak at $E_x=17.1$ MeV, which lies on the top of the considerable amount of the leftover unperturbed strength in the same energy region. The small peak is difficult to recognize in the IV response, if it is calculated without including the IS RPA correlation. Thus, the small peak can be regarded as the IV strength due to the neutron excess, which is brought to the energy region of the IS GMR. However, the ratio of the IV strength to the IS strength at the IS GMR is much smaller than the value of $(N-Z)/A$, which is the approximate ratio for the IV quadrupole strength found at the IS GQR [11] due to the same neutron excess.

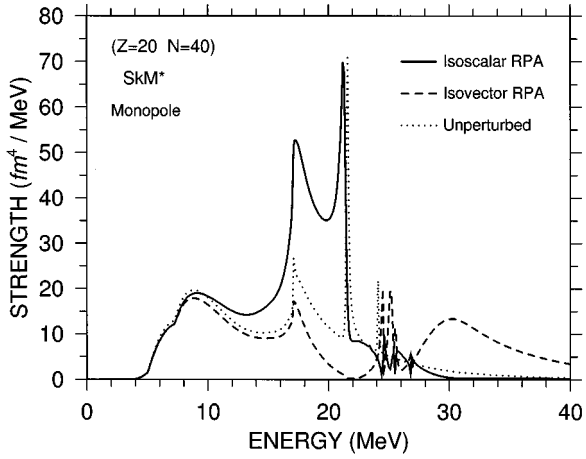

FIG. 12. RPA monopole strength function of ^{60}Ca as a function of excitation energy. The SkM* interaction is used consistently both in the HF and the RPA calculations. The IS (IV) response is shown by the solid (dashed) curve, while the unperturbed response is denoted by the dotted curve.

The IS transition densities at various excitation energies are shown in Figs. 13(a) and 13(b). The $B(\lambda=0)$ values of the densities are normalized to be 25.1, 33.3, and 78.9 fm^4 for $E_x=7.0$, 11.0, and 17.2 MeV, respectively. The transition densities at the low energy peaks in Fig. 13(b) are entirely dominated by neutron excitations. The transition densities of those threshold strength at lower energies have a longer tail far outside of the nuclear surface. The IS transition density of the high energy peak at $E_x=17.2$ MeV in Fig. 13(a) consists of a comparable amount of the proton and the neutron contributions, and the radial dependence is similar to the Tassie transition density. In Fig. 13(c) we show the displacement field (10) calculated at an energy of the threshold strength, $E_x=7.0$ MeV. It is seen that the displacement field of neutrons is small inside of the nucleus and is steeply rising outside, while that of protons is negligible everywhere. For reference, the displacement field calculated numerically by using the Tassie transition density is plotted, in which the Tassie density is normalized so as to give the same $B(\lambda=0)$ value. The displacement field of protons and that of neutrons in the IS GMR energy region ($14<E_x<22$ MeV) depend rather sensitively on the value of E_x and are not very similar to each other as a function of r.

The RPA IS responses of four Ca isotopes are shown in Fig. 14(a). A considerable amount of the proton strength in ^{34}Ca and that of the neutron strength in ^{60}Ca, which lie in the energy region of $E_x=4-12$ MeV, express the threshold strength that is a characteristic feature of the response in drip line nuclei. The calculated RPA IS strength extends over a large energy range, especially in drip line nuclei ^{34}Ca and ^{60}Ca, but also in β-stable nuclei ^{40}Ca and ^{48}Ca. The IS monopole response in all Ca isotopes is far away from a single peak, which is a clear manifestation of the collective vibration. The integrated area under each curve is equal to the IS EWSR, $m_1=2\hbar^2A\langle r^2\rangle_m/m$, and is an increasing function of the mass number.

The RPA IV responses of four Ca isotopes calculated using the SkM* interaction are shown in Fig. 14(b). Since the threshold strength in the energy region of $E_x=4-12$ MeV of

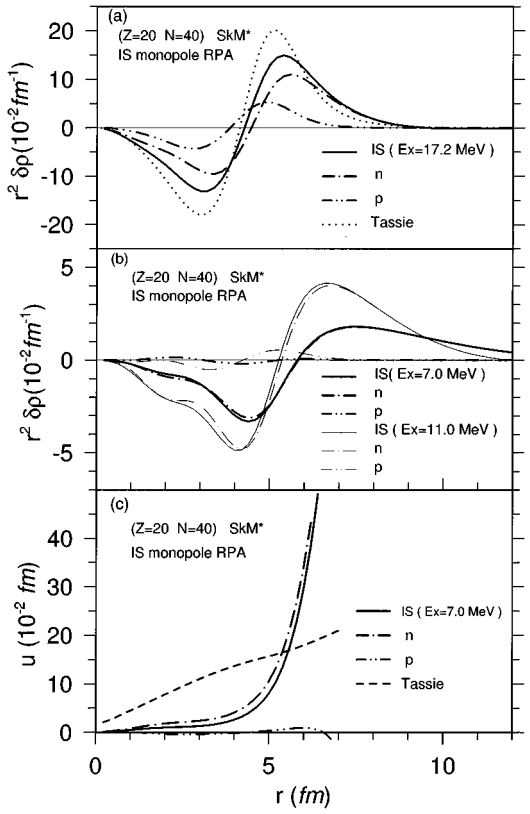

FIG. 13. Radial transition densities of the IS response in ^{60}Ca as a function of radial coordinate: (a) at an energy $E_x = 17.2$ MeV, which is inside of the broad bump of the IS GMR; (b) at energies $E_x = 7.0$ and 11.0 MeV, which are much lower than that of the IS GMR. The SkM* interaction is used. The neutron part is shown by dot-dashed lines, while the proton part is denoted by dot-dot-dashed lines. The IS density is expressed by solid lines, while the Tassie density for GMR (8) by the dotted curve in (a), which is normalized so as to give the same $B(\lambda = 0)$ value as that of the IS density at $E_x = 17.2$ MeV. (c) The displacement field (10) calculated at an energy of the threshold strength, $E_x = 7.0$ MeV. For reference, the displacement field, which is numerically calculated using the Tassie transition density, is plotted by the dashed line. The Tassie transition density is normalized so as to give the same $B(\lambda = 0)$ value as that of the plotted IS transition density at $E_x = 7.0$ MeV.

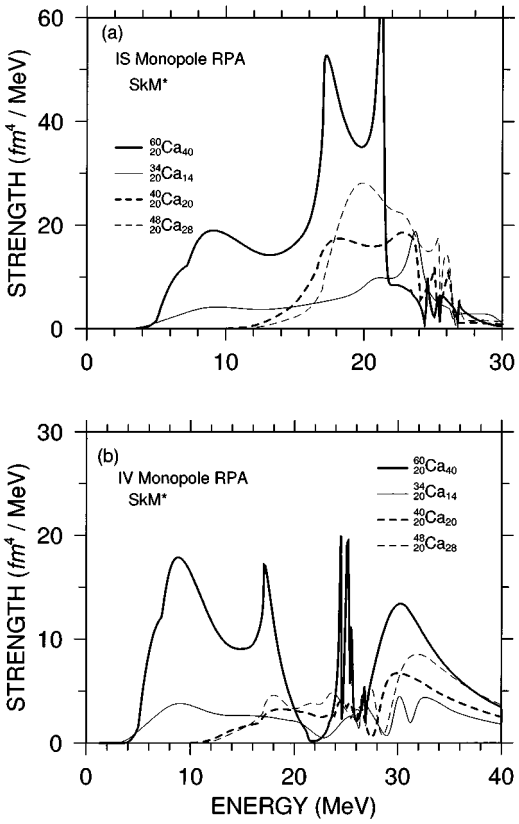

FIG. 14. (a) RPA IS monopole strength of Ca isotopes. (b) RPA IV monopole strength of Ca isotopes. The RPA response functions of ^{34}Ca, ^{40}Ca, ^{48}Ca, and ^{60}Ca are given by thin solid, thick dashed, thin dashed, and thick solid lines, respectively. The SkM* interaction is used.

^{34}Ca and ^{60}Ca consists exclusively of the proton and the neutron excitations, respectively, the RPA IV strength is nearly the same as the respective unperturbed strengths. The major part of the IV strength in the region of $E_x \approx 12-30$ MeV is the leftover unperturbed strength, which is not shifted to a higher energy region by the IV RPA correlation. The IV GMR is identified as a large bump at $E_x > 30$ MeV, of which the strength is clearly shifted from the low energy region of the unperturbed strength. Very little IS strength is seen in the region of the IV GMR.

Calculated energies E_0^s, E_0^c, and E for Ca isotopes are given in Table III together with the compression moduli K_A^s and K_A^c and the variance σ. Due to the large transition strength just above the threshold of ^{34}Ca and ^{60}Ca, the literally calculated value of the variance σ is large in these two nuclei compared with the variance in ^{40}Ca and ^{48}Ca. It is not clear how seriously those literally estimated compression moduli, K_A^s and K_A^c, should be taken, since in these Ca isotopes the calculated IS GMR is far away from a single collective vibration.

V. DYNAMICAL STRUCTURE OF CONTINUUM STATES

A number of excitations with different dynamical structure may in general coexist at a given excitation energy in the continuum. For example, at a given excitation energy one may find both the IS and the IV collective strength, of which the form factors of the excitations are totally different from each other. This is in contrast to an isolated quantum state such as bound-state excitations, of which the width is negligibly small compared with level distances. In $N = Z$ nuclei it is trivial to separate the IS and the IV excitations, even in the continuum, since they have different isospins. On the other hand, in nuclei with $N \gg Z$ (or $N \ll Z$) the IS and the IV excitations at a given energy may have the same isospin in a good approximation, and the coexistence of the two types of excitations is an interesting problem.

Our present way of treating the continuum can naturally provide different neutron (proton) form factors for the IS and the IV excitations, even when they may occur at the same excitation energy. In contrast, if a state in the continuum is approximated by using the basis expansion with a finite set of oscillator wave functions, the neutron part and the proton part of the resulting wave function are fixed and, thus, the

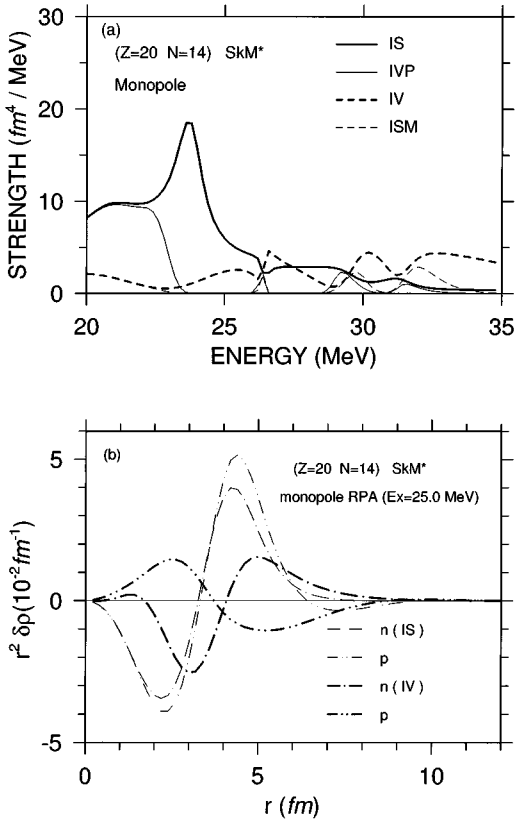

FIG. 15. (a) Monopole response functions of ^{34}Ca as a function of excitation energy, which are calculated by using the RPA IS transition densities, $\delta\rho^n_{\rm IS}$ and $\delta\rho^p_{\rm IS}$, and the RPA IV transition densities, $\delta\rho^n_{\rm IV}$ and $\delta\rho^p_{\rm IV}$. The monopole strengths estimated using $\delta\rho^n_{\rm IS}(\vec{r})+\delta\rho^p_{\rm IS}(\vec{r})$, $\delta\rho^n_{\rm IV}(\vec{r})-\delta\rho^p_{\rm IV}(\vec{r})$, $\delta\rho^n_{\rm IS}(\vec{r})-\delta\rho^p_{\rm IS}(\vec{r})$, and $\delta\rho^n_{\rm IV}(\vec{r})+\delta\rho^p_{\rm IV}(\vec{r})$, are denoted by thick solid lines (IS), thick dashed lines (IV), thin dashed lines (ISM), and thin solid lines (IVP), respectively. The SkM* interaction is used. (b) RPA radial transition densities at $E_x=25.0$ MeV, which are estimated using the SkM* interaction. The neutron (proton) part of the IS transition density is expressed by thin dot-dashed (thin dot-dot-dashed) lines, while the neutron (proton) part of the IV transition density by thick dot-dashed (thick dot-dot-dashed) lines.

form factors of the IS and the IV excitation are uniquely related to each other. In Refs. [8] and [11] we studied this problem in the continuum for quadrupole excitations in nuclei with a large neutron (or proton) excess, using the present HF+RPA model. We have found that both the neutron and proton parts of the IS transition density are nearly equal to the respective part of the IV transition density at the same energy of the quadrupole response, almost whenever appreciable amounts of both the IS and the IV quadrupole strength are found at the given energy. In the present section we demonstrate a numerical example of monopole responses, which at a given energy in the continuum shows the coexistence of excitations with a different dynamical structure.

TABLE III. Calculated properties of the IS RPA response in Ca isotopes. All values are calculated by using the SkM* interaction. See the captions to Table I.

A	E_0^s (MeV)	$\overline{E}$ (MeV)	E_0^c (MeV)	K_A^s (MeV)	K_A^c (MeV)	σ (MeV)	$\sqrt{\langle r^2\rangle_m}$ (fm)
^{34}Ca	22.5	19.4	17.8	132.0	82.9	6.6	3.294
^{40}Ca	22.0	20.8	20.5	135.0	117.0	4.0	3.402
^{48}Ca	22.6	21.6	21.4	154.0	138.0	3.6	3.541
^{60}Ca	18.8	16.5	15.4	132.0	88.5	5.3	3.934

Expressing the neutron (proton) part of the IS transition density by $\delta\rho^n_{\rm IS}$ ($\delta\rho^p_{\rm IS}$) and that of the IV one by $\delta\rho^n_{\rm IV}$ ($\delta\rho^p_{\rm IV}$), the measurable reduced transition probability is written as

$$B(\lambda,\tau=0{:}0\rightarrow n)=\sum_\mu \left| \int [\,\delta\rho^n_{\rm IS}(\vec{r})+\delta\rho^p_{\rm IS}(\vec{r})]Q^{\lambda\,\tau=0}_\mu d^3r \right|^2 \tag{24}$$

and

$$B(\lambda,\tau=1{:}0\rightarrow n)=\sum_\mu \left| \int [\,\delta\rho^n_{\rm IV}(\vec{r})-\delta\rho^p_{\rm IV}(\vec{r})]Q^{\lambda\,\tau=1}_\mu d^3r \right|^2. \tag{25}$$

Now, using the calculated transition densities, $\delta\rho^n_{\rm IS}$, $\delta\rho^p_{\rm IS}$, $\delta\rho^n_{\rm IV}$, and $\delta\rho^p_{\rm IV}$, we may define

$$C(\lambda,\tau=0{:}0\rightarrow n)=\sum_\mu \left| \int [\,\delta\rho^n_{\rm IV}(\vec{r})+\delta\rho^p_{\rm IV}(\vec{r})]Q^{\lambda\,\tau=0}_\mu d^3r \right|^2 \tag{26}$$

and

$$C(\lambda,\tau=1{:}0\rightarrow n)=\sum_\mu \left| \int [\,\delta\rho^n_{\rm IS}(\vec{r})-\delta\rho^p_{\rm IS}(\vec{r})]Q^{\lambda\,\tau=1}_\mu d^3r \right|^2. \tag{27}$$

If a continuum state contains only one dynamical structure instead of two different correlations of the IS and the IV type, we have $\delta\rho^n_{\rm IS}(\vec{r})=\delta\rho^n_{\rm IV}(\vec{r})$ and $\delta\rho^p_{\rm IS}(\vec{r})=\delta\rho^p_{\rm IV}(\vec{r})$. Thus, we should have $C(\lambda,\tau=0{:}0\rightarrow n)=B(\lambda,\tau=0{:}0\rightarrow n)$ and $C(\lambda,\tau=1{:}0\rightarrow n)=B(\lambda,\tau=1{:}0\rightarrow n)$. This is the case typical of the threshold strength in drip line nuclei or the IS giant quadrupole resonance (GQR) in nuclei with neutron (or proton) excess [8]. In contrast, if for a given energy both $B(\lambda,\tau=0{:}0\rightarrow n)$ and $B(\lambda,\tau=1{:}0\rightarrow n)$ have appreciable values while both $C(\lambda,\tau=0{:}0\rightarrow n)$ and $C(\lambda,\tau=1{:}0\rightarrow n)$ are negligibly small, it indicates that two excitation modes (IS and IV) with almost independent dynamical structure exist at that energy. The occurrence of this situation depends on nuclei and multipoles, and may not particularly be unique in drip line nuclei.

In Fig. 15(a) we show the RPA monopole response functions of $^{34}_{20}$Ca$_{14}$, which are estimated using the transition densities, $\delta\rho^n_{\rm IS}(\vec{r})+\delta\rho^p_{\rm IS}(\vec{r})$, $\delta\rho^n_{\rm IV}(\vec{r})-\delta\rho^p_{\rm IV}(\vec{r})$, $\delta\rho^n_{\rm IS}(\vec{r})-\delta\rho^p_{\rm IS}(\vec{r})$, and $\delta\rho^n_{\rm IV}(\vec{r})+\delta\rho^p_{\rm IV}(\vec{r})$, and are expressed by thick solid lines, thick dashed lines, thin dashed lines, and thin solid lines, respectively. The thick solid lines and the thick dashed lines are identical to the respective lines in Fig. 10. In Fig. 15(a) it is seen that around $E_x=25.0$ MeV both thin lines are negligibly small, while both thick lines have appreciable values. In Fig. 15(b) we show the calculated radial transition densities at the energy, $E_x=25.0$ MeV. It is nicely seen that the radial transition densities $\delta\rho^n_{\rm IS}(r)$ and

$\delta\rho^{p}_{\rm IS}(r)$ are in phase and similar as a function of the radial coordinate, while $\delta\rho^{n}_{\rm IV}(r)$ and $\delta\rho^{p}_{\rm IV}(r)$ are out of phase with each other. Moreover, the radial dependence of the IS transition densities is clearly different from that of the IV ones. The results shown in Fig. 15 at $E_x=25.0$ MeV demonstrate the coexistence of two independent excitations at the same energy in the continuum.

VI. SUMMARY

We study the giant monopole resonances in stable nuclei ^{40}Ca, ^{90}Zr, and ^{208}Pb, and the drip line nuclei of Ca isotopes, using the self-consistent HF calculation plus the RPA with Skyrme interactions, SkM*, SGI, and SIII. The RPA response function is calculated in the coordinate space so as to take properly into account the continuum effect, including simultaneously both the isoscalar and the isovector correlation. We found that in both proton and neutron drip line nuclei the distribution of the monopole strength is greatly affected by the presence of the low-energy threshold strength, while in the β-stable heavy nucleus ^{208}Pb the IS monopole strength is, in a good approximation, concentrated on a single peak. In lighter β-stable nuclei such as ^{40}Ca the major part of the RPA IS strength stays in the same energy region as that of the unperturbed strength and, thus, the IS GMR is not realized as a single collective peak. A certain amount of the unperturbed IV strength is not shifted by the RPA correlations to the higher energy region of the IV GMR, but it remains in the original unperturbed energy region even in the case of ^{208}Pb. The remaining portion is larger in lighter β-stable nuclei, and it is even larger in drip line nuclei due to the presence of the low-energy threshold strength.

The transition densities of the IS GMR are in fair agreement with those given by the collective Tassie model, while the transition densities of the threshold strength in drip line nuclei have a very different radial dependence from that of the Tassie model. In both β-stable and drip line nuclei the transition density of the IV GMR differs considerably from that of either the Tassie or the hydrodynamical polarization model.

Using our present model, the relation between the compression modulus of nuclear matter K_{nm} and that of finite nuclei K_A in Eq. (13) is discussed employing the RPA result of β-stable nuclei, ^{40}Ca, ^{90}Zr, and ^{208}Pb, with three different Skyrme forces. The analysis indicates that even ^{208}Pb is not large enough to obtain a proportionality relation between K^{s}_{A} and K_{nm}.

The GMR in the proton drip line nucleus ^{34}Ca and the neutron drip line nucleus ^{60}Ca is studied using the SkM* interaction, in comparison with the β-stable nuclei ^{40}Ca and ^{48}Ca. The IS monopole strength of the RPA solutions in Ca isotopes remains in the same energy region as that of the unperturbed strength, though the shape of the strength distribution is changed by the RPA correlation. Namely, the unperturbed strength in the drip line nuclei is extended over a very broad region of $5<E_x<30$ MeV, as does the IS RPA strength. In ^{34}Ca the low-lying threshold strength is entirely due to proton excitations, while in ^{60}Ca it consists exclusively of neutron excitations. The transition densities of the low energy threshold strength have a node outside of the nuclear surface and, then, an extended tail due to the proton (neutron) skin with small binding energies in ^{34}Ca (^{60}Ca). The IV strength just above the threshold of drip line nuclei is naturally almost equal to the IS strength. An appreciable amount of the IV strength is found in the region of $E_x<30$ MeV, which is the remaining unperturbed strength without being shifted by the IV RPA correlation. The correlated IV GMR is identified as a clear peak above $E_x\approx 30$ MeV.

The displacement fields are discussed in both the β-stable nucleus ^{208}Pb and the drip line nuclei, ^{34}Ca and ^{60}Ca. The displacement field of the IS GMR in ^{208}Pb has almost equal contributions from protons and neutrons and shows a radial dependence similar to that of the Tassie model. On the other hand, in drip line nuclei the displacement field of protons behaves differently from that of neutrons, especially around the nuclear surface.

Excitations with different dynamical structure but with the same quantum numbers may in general coexist at a given energy in the continuum. Using our present HF+RPA model, we have demonstrated that in the monopole response of ^{34}Ca the two excitations of almost pure IS and IV character, respectively, coexist at the same energy, while having different transition densities.

ACKNOWLEDGMENTS

One of the authors (X.Z.Z.) acknowledges the financial support provided by the Wenner-Gren Foundation, which makes it possible for him to work at the Lund Institute of Technology. This work was partially supported by the Grant in Aids for the Scientific Research by Japanese Ministry of Education, Science, Sports and Culture under Contract No. 09640369.

[1] J. P. Blaizot, Phys. Rep. **64**, 171 (1980).
[2] O. Bohigas, A. M. Lane, and J. Martorell, Phys. Rep. **51**, 267 (1979).
[3] H. Krivine, J. Treiner, and O. Bohigas, Nucl. Phys. **A336**, 155 (1980).
[4] J. Treiner, H. Krivine, O. Bohigas, and J. Martorell, Nucl. Phys. **A371**, 253 (1981).
[5] M. M. Sharma *et al.*, Phys. Rev. C **38**, 2562 (1988).
[6] N. Auerbach, Phys. Rep. **98**, 273 (1983); T. Suzuki, H. Sagawa, and G. Còlo, Phys. Rev. C **54**, 2954 (1996).
[7] I. Hamamoto, H. Sagawa, and X. Z. Zhang, Phys. Rev. C **53**, 765 (1996); I. Hamamoto and H. Sagawa, *ibid.* **53**, R1492 (1996).
[8] I. Hamamoto, H. Sagawa, and X. Z. Zhang, Phys. Rev. C **55**, 2361 (1997).
[9] Nguyen van Giai and H. Sagawa, Nucl. Phys. **A371**, 1 (1981).

[10] J. P. Blaizot, J. F. Berger, D. Decharge, and M. Girod, Nucl. Phys. **A591**, 435 (1995).
[11] I. Hamamoto, H. Sagawa, and X. Z. Zhang, Nucl. Phys. A (in press).
[12] A. Bohr and B. R. Mottelson, *Nuclear Structure* (Benjamin, New York, 1975), Vol. II, p. 670.
[13] B. K. Jenning and A. D. Jackson, Phys. Rep. **66**, 141 (1980).
[14] S. Brandenburg, R. De Leo, A. G. Drentje, M. N. Harakeh, H. Sakai, and A. van der Woude, Phys. Lett. **130B**, 9 (1983).
[15] D. H. Youngblood, Y.-W. Lui, and H. C. Clark, (unpublished).
[16] J. M. Blatt and V. F. Weisskopf, *Theoretical Nuclear Physics* (Wiley, New York, 1952).
[17] D. H. Youngblood *et al.*, Phys. Rev. C **23**, 1997 (1981).
[18] W. T. A. Borghols *et al.*, Nucl. Phys. **A504**, 231 (1989).
[19] M. Buenerd, in *Proceedings of the International Symposium on Highly Excited States and Nuclear Structure*, edited by N. Marty and Nguyen Van Giai [J. Phys. (Paris), Colloq. **45**, C4-115 (1984), and references therein].
[20] S. Brandenburg *et al.*, Nucl. Phys. **A466**, 29 (1987).